Supporting Information

Promotion of Homogeneous Ice Nucleation by Soluble Molecules

Kenji Mochizuki,[1,2] Yuqing Qiu,[1] and Valeria Molinero[1]

[1]Department of Chemistry, The University of Utah, Salt Lake City, Utah 84112-0580, USA

[2]Research Institute for Interdisciplinary Science, Okayama University, Okayama 700-8530, Japan

Contents

A. Models

Water was represented by the monoatomic water model mW,[1] which reproduces the structures, thermodynamics, and phase behavior of water[1-4] and aqueous solutions[5-7] at less than 1% of the computational cost of fully atomistic models. Polyvinyl alcohol (PVA) was represented by a recently developed united atom model.[8] The interactions between the hydrocarbon groups of PVA (CH_3, CH_2, and CH) were modeled with single sites interacting through the Lennard-Jones potential with the parameters of the UA-OPLS force field.[9] The cross interaction between the hydrocarbon sites and the mW water was tuned in ref. [8] to reproduce the experimental radii of gyration of PVA as a function of its degree of polymerization. The interaction between the OH groups was represented by a single particle with interactions identical to those in the mW model. We summarize these pair interactions in Table S1.

Table S1. The parameters [ε (kcal mol^{-1}), σ (Å)] for Lenanrd-Jones interactions. mW indicates that the parameters are those of the monatomic water model mW.[1]

	CH_3	CH_2	CH	OH	H_2O
CH_3	0.175, 3.905	---	---	---	---
CH_2	0.118, 3.877	0.118, 3.905	---	---	---
CH	0.144, 3.905	0.097, 3.877	0.080, 3.850	---	---
OH	0.170, 3.536	0.170, 3.536	0.170, 3.536	mW	---
H_2O	0.204, 3.536	0.204, 3.536	0.204, 3.536	mW	mW

The bond lengths were constrained using harmonic bond potentials; $U(r) = K(r - r_0)^2$, where K = 30 kcal mol^{-1} Å^{-2} and r_0 = 1.53 Å for all C-C bonds, and K = 30 kcal mol^{-1} Å^{-2} and r_0 = 1.43 Å for the CH-OH bond.[17] The angles were constrained using harmonic angle potentials; $U(r) = L(\theta - \theta_0)^2$, where L = 30 kcal mol^{-1} radian^{-2} and θ_0 = 108° for CH_3-CH-CH_2, CH_3-CH-OH and CH_2-CH-CH_2, L = 30 kcal mol^{-1} radian^{-2} and θ_0 = 112° for OH-CH-CH_2, CH-CH_2-CH and CH_2-CH-OH.[17] All dihedral potentials were the same; $U(r) = K_1(1 + cos\phi)/2 + K_2[(1 - cos(2\phi)]/2 + K_3[(1 + cos(3\phi)]/2 + K_4[(1 - cos(4\phi)]/2,$ where K_1 = 1.411 kcal mol^{-1}, K_2 = -0.271 kcal mol^{-1}, K_3 = 3.145 kcal mol^{-1} and K_4 = 0.0 kcal mol^{-1}.[8]

B. Systems

We prepared cubic simulation cells of aqueous solutions containing PVA molecules with three different degrees of polymerization: monomer, 5-mer and 10-mer. The simulation cells contained 4608 water molecules. The number of PVA molecules (N_{PVA}) in the simulation cells was 10, 20 or 50 for PVA monomer solutions, corresponding to PVA concentration of 0.72, 1.43 and 3.49 wt%,

respectively, N_{PVA}= 2 (0.57 wt%), 5 (1.40 wt%) and 30 (7.86 wt%) for 5-mer solutions, and N_{PVA}=1 (0.55 wt%), 3 (1.62 wt%) and 15 (7.62 wt%) for 10-mer solutions. The PVA 10-mer solution with concentration 0.55 wt% was used for the analyses presented in Fig. 2.

C. Molecular dynamics simulations

Molecular dynamics (MD) simulations were carried out using LAMMPS,[10] integrating the equations of motion with the velocity-verlet algorithm using a time step of 5 fs. The temperature (T) and pressure (p) were controlled with the Nose-Hoover thermostat and barostat at 1 atm, with damping constants 2.5 and 12.5 ps, respectively. Periodic boundary conditions were applied to the three directions. The initial configurations of the solutions were prepared with PVA randomly located in the simulation cell. Then, the system was relaxed through energy minimization using the Polak-Ribiere version of the conjugate gradient algorithm, followed by MD simulations in the canonical (*NVT*) and isobaric isothermal (*NpT*) ensembles. The *NpT*-MD simulations were performed to obtain freezing trajectories (Figs. 1A and 2B) as well as the statistical distributions of PVA and liquid water around an ice embryo (Figs. 2C and 2D). Grand canonical MD simulations were performed to compute the activity of water in PVA solutions (Fig. 1B). The details of simulations are described in the following sections.

D. Crystallization of ice

Each PVA solution was equilibrated for 250 ps of *NVT* simulation at 400 K, followed by 5 ns of *NpT* simulation at 250 K. Then, the system was cooled down at a rate of -0.2 K ns^{-1} from 220 to 195 K. For each PVA concentration, we performed at least 20 (70 for 0.55 wt% PVA 10-mer solution) independent freezing trajectories, starting the cooling protocol from the same equilibrated configuration with different distribution of velocities. The freezing temperature T_x corresponds to the inflection point in the fraction of ice, where the ice was identified by the CHILL+ algorithm.[11] We define the freezing efficiency of the solution as $\Delta T_x \equiv T_x - T_x^0$, where with T_x^0 is the freezing temperature of pure water ($T_x^0 = 201.8 \pm 2.2$ for mW water at the cooling rate of the simulations).

E. Equilibrium distributions of PVA and liquid water around the ice embryo

First, we replicated the crystalline structure of ice I_h in the whole cell and selected a group of water molecules within 0.89 nm from an arbitrary molecule. This results in an ice cluster with 99 water molecules. Second, we applied a harmonic force independently to each of the selected molecules to tether them to their initial position, where the spring constant is 10.9 kcal mol^{-1} Å^{-2}. Then, we performed a 50 ps *NpT* simulation at 275 K to melt the ice structure surrounding the constrained molecules. After the equilibration, we performed a 800 ns long *NpT* simulation at 275 K to obtain the

statistical distribution of a single PVA 10-mer around the ice nucleus. The temperature of 275 K was chosen to prevent the growth of ice embryo, because the equilibrium melting temperature of mW model is $T_m = 273 \pm 0.5$ K.[12] Using this trajectory, we computed the equilibrium number density distributions of liquid water and PVA-OH as a function of the distance from center of mass of the ice embryo (Figs. 2C and 2D).

F. Comparison between equilibrium and non-equilibrium distributions of PVA around the ice nucleus

The precise distribution of PVA and liquid water around an ice embryo is necessary to compute the effect of PVA on the ice-water surface tension. However, the crystallization of ice is stochastic and very fast; hence there is only one configuration per simulation in which the ice embryo has a critical size. Instead, we computed the distribution of PVA-OH (of 10-mer) around the ice nucleus, which should be critical when it has around 100 water molecules, and found it to be almost the same in equilibrium and non-equilibrium simulations (Figure S1). The equilibrium distribution was computed as described in S1-5. The non-equilibrium distribution was computed from 70 independent freezing trajectories. The ice nucleus size of the sampled configurations is 105±37 molecules.

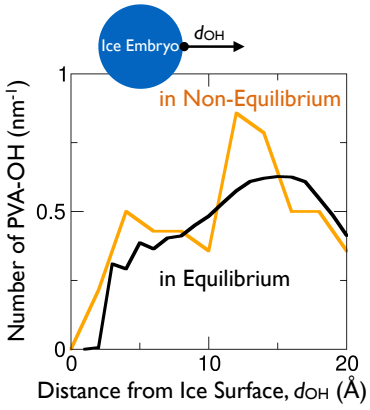

Figure S1. Distributions of PVA-OH around an ice embryo with ~100 molecules as a function of the distance from the surface of ice embryo (d_{OH}), computed for PVA 10-mer solution of 0.55 wt% in equilibrium (orange) and non-equilibrium (black) simulations.

G. Effect of PVA on the ice-liquid surface tension using Gibbs adsorption isotherm[13]

The Gibbs adsorption isotherm is a relationship between the surface tension and excess surface concentrations. For example, it is well known that the surface tension of oil in water decreases when a surfactant is added. Likewise, a molecule that is a surfactant to the ice-liquid interface would decrease the ice-liquid surface tension. The surface excess of liquid water is expressed as

$$\Gamma_{liq} = \int_0^z \rho_{liq}(z)dz + \int_z^{+\infty} \left[\rho_{liq}(z) - \rho_{liq}(\infty)\right] dz,$$

where $\rho_{liq}(z)$ is the density profile of liquid water as a function of the distance z from the center of mass of the ice embryo (Fig. 2C) and $\rho_{liq}(\infty)$ is the bulk liquid density. We chose the position of the ice-liquid Gibbs dividing plane such that $\Gamma_{liq} = 0$ (the dashed line in Figs. 2C and 2D). The Gibbs adsorption equation sets a relationship between the surface excess Γ_{PVA}^{liq} of PVA at the ice-liquid Gibbs dividing surface and the change of the ice-liquid surface tension $\gamma_{ice-liq}$ with the activity of PVA a_{PVA}:

$$\Gamma_{PVA}^{liq} = -\frac{a_{PVA}}{RT}\frac{\partial \gamma_{ice-liq}}{\partial a_{PVA}},$$

where R and T are the gas constant and temperature, respectively. Then, we compute the change of ice-liquid surface tension $\Delta\gamma_{ice-liq}$ with respect to that between ice and pure water as a function of Γ_{PVA}^{liq}:

$$\Delta\gamma_{ice-liq} \simeq -RT\Gamma_{PVA}^{liq}. \qquad \text{(S1)}$$

We follow the procedure based eq. 1 to compute the change Δγ in surface tension for the ice-liquid interface in the presence of PVA. Although the location of ice-liquid Gibbs dividing surface (Figure 2d of the main text) depends on the identification of ice and liquid in the simulations, we verify that a few angstroms shift of the ice-liquid interface does not significantly change Δγ.

We verify the accuracy of equation S1 through the calculation of liquid-vapor surface tension of PVA 5-mer solutions, computed through the pressure tensors:[14]

$$\gamma_{liq-vap} = \frac{1}{2}L_z \langle P_{zz} - \frac{1}{2}\left(P_{xx} + P_{yy}\right)\rangle,$$

where L_z is the length of the simulation box along the direction perpendicular to the liquid-vapor interface, P_{zz} is the normal component of the pressure tensor, P_{xx} and P_{yy} are the tangential components of the pressure tensor, and $\langle \ldots \rangle$ indicates the time average. The pressure tensor route is valid only for the calculation of the surface tensions of fluid-fluid interfaces, cannot be applied to the calculation of the ice-liquid surface tension.

NVT simulations, each 400 ns long, were performed for pure water and two different concentrations of PVA 5-mer solutions, contained in a $156\ \text{Å} \times 52\ \text{Å} \times 52\ \text{Å}$ rectangular box (Figure S2A). The simulation cells contained 4608 molecules, and 10 or 30 molecules, respectively, of PVA 5-mer. The

z-axis dependent number densities of PVA-OH and water molecules (Figure S2B) were used to compute the surface tension through Eq. S1. Figure S2C demonstrates that the two different ways give the same result for the liquid-vapor surface tension of PVA solutions.

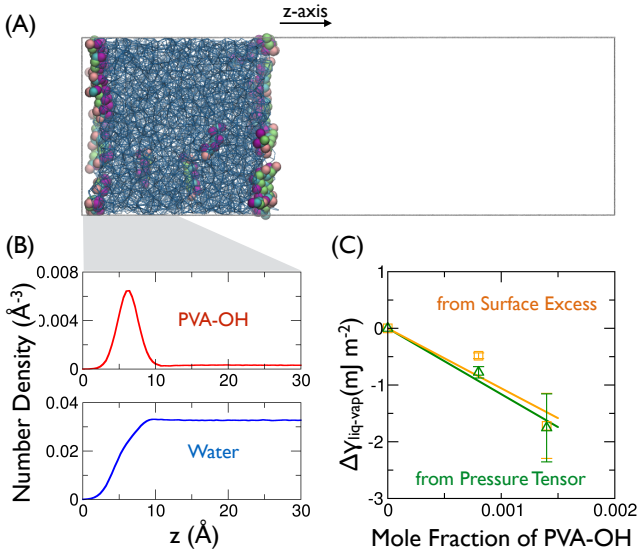

Figure S2. (A) A snapshot of PVA 5-mer solution consisting 4608 water and 30 PVA molecules, (B) Distribution of PVA-OH (red) and water (blue) molecules as a function of z, (C) The change in liquid-vapor surface tension computed from pressure tensors (green) and surface excesses (orange). The PVA-OH mole fraction is the averaged value in the bulk region.

H. Water activity in PVA solutions

Coarse-grained models based on short-ranged potentials can quantitatively reproduce the experimental water activity a_w in NaCl and LiCl solutions over a wide range of concentrations.[15] We use grand canonical molecular dynamics simulations to compute the activity of water in PVA solutions, following the procedures of ref. [15]. The models and number of molecules are the same as mentioned in Sec. A and B. The temperature was set to 275 K. First, we performed 5 ns long NpT simulations to equilibrate each PVA solution at p = 0 atm. Then, a series of grand canonical (μVT) MD simulations, each 45 ns long, were carried out at different chemical potentials of water (which correspond to different values of vapor pressures, p_v). Figure S3 shows the relationship between the mechanical pressure of PVA solution and the vapor pressure p_v of water. When the mechanical pressure is equal to the equilibrium vapor pressure (which we approximate to 0 atm for the fitting), then the solution is in equilibrium and we read from the graph the activity of water, $a_w = p_v/p_v^*$, where p_v^* is the pressure of pure water.

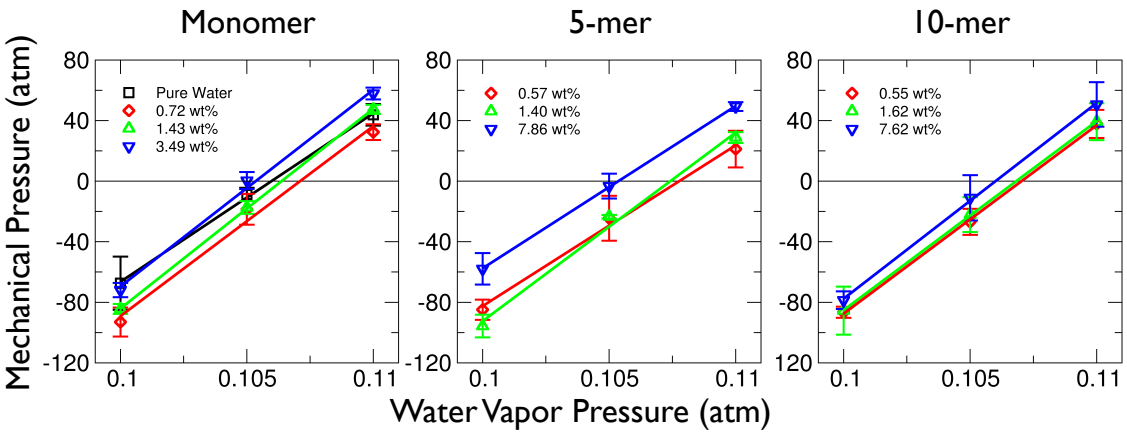

Figure S3. Mean values of mechanism pressure of PVA solutions as a function of the vapor pressure p_v of water for the aqueous solutions of PVA monomer, 5-mer and 10-mer at 275 K. The equilibrium water activity is the one for which the mechanical pressure equals the vapor pressure.

The activity coefficient of water, γ_w, measures the non-ideal interactions in the solution, and is defined as the ratio between the activity a_w and the mole fraction x_w of water in the PVA solution; $\gamma_w = a_w/x_w$. Figure S4 shows that the activity coefficients are always larger than one, *i.e.* repulsive, and a non-monotonous function of PVA concentration, reaching a maximum at about the same concentration that the activity presents a maximum.

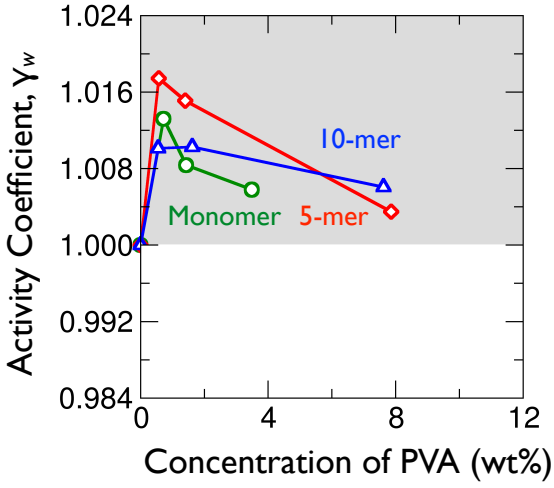

Figure S4. Activity coefficients γ_w for PVA monomer, 5-mer and 10-mer solutions as a function of the concentration of PVA for the solutions at 275 K.

I. Influence of hydrophobicity on the freezing efficiency of PVA

The non-ideal repulsive interactions evinced by $\gamma_w > 1$ suggest that the increase in water activity in the presence of small concentrations of PVA is due to the repulsive character of the interactions of water with the hydrophobic groups in the molecule. In order to examine the influence of hydrophobicity on the freezing efficiency ΔT_x, we weaken the strength of the Lennard-Jones interaction ε between the hydrocarbon groups of PVA and the water molecules in a 0.55 wt% 10-mer solution, which contains only one PVA 10-mer. Figure S4 shows that the freezing efficiency increases with decreasing the carbon-water interaction (increasing the hydrophobicity). The result confirms that the hydrophobic moiety of PVA destabilizes the liquid water and increases the activity in the PVA solutions.

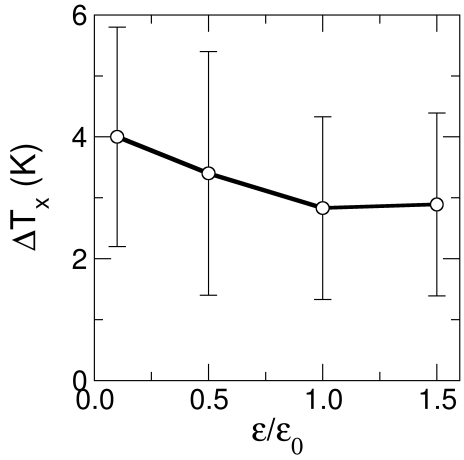

Figure S5. Freezing efficiency ΔT_x as a function of $\varepsilon/\varepsilon_0$, where ε_0 is the original value presented in Table S1.

J. Prediction of the effect of water activity on the homogeneous freezing temperature using the parameterizations derived for $a_w < 1$.

We predict the effect of water activity on the rise in homogeneous ice nucleation temperature of the solution, $\Delta T_x = T_x^{solution} - T_x^{water}$ by extrapolation to $a_w > 1$ of the empirical analytical equations for $T_x(a_w)$ fitted in the range of $a_w < 1$ using experiments[20] and simulations with mW water.[21] This results in the two solid lines shown in Figure S6. The agreement between this approach and the results of the simulations (Figure 3 of main text) indicates that this is a reliable way to predict the effect of water activity on the freezing efficiency of solutions. Interestingly, the predictions from the simulations and experiment are in excellent agreement, which is surprising considering that the rates of nucleation in both cases are quite different, $J \approx 10^5$ cm^{-3} s^{-1} in the experiments that produce T_{hom} = 238 K for pure water, and $J \approx 10^{24}$ cm^{-3} s^{-1}, given by the cooling rate, in the simulations). The

agreement indicates that it is possible to use freezing simulations with mW to accurately predict the effect of water activity on the freezing efficiency ΔT_x of solutions, provided that the model captures the activity of the solutions.

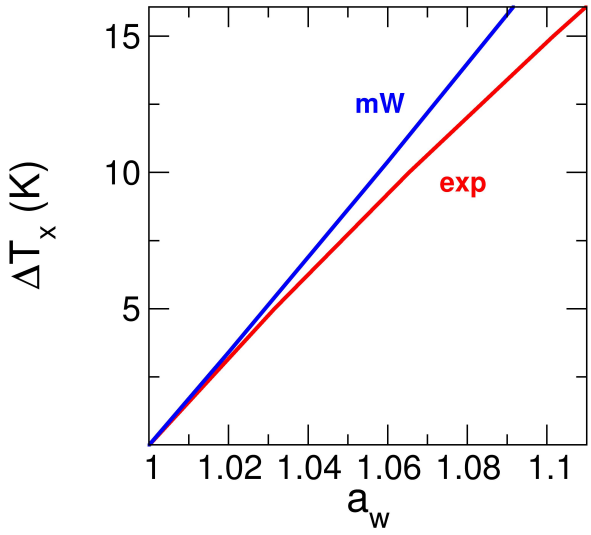

Figure S6. Freezing efficiency ΔT_x as a function of water activity a_w. The lines show the extrapolations to $a_w > 1$ of the parameterizations of $\Delta T_x(a_w)$ by Koop et al. based on experimental data[20] (red) and by Bullock and Molinero based on simulations with the mW water models (blue).[21]

References

(1) Molinero, V.; Moore, E. B. *J. Phys. Chem. B* **2009**, 113, 4008-4016.

(2) Malkin, T. L.; Murray, B. J.; Salzmann, C. G.; Molinero, V.; Pickering, S. J.; Whale, T. F. *Phys. Chem. Chem. Phys.* **2015**, 17, 60-76.

(3) Moore, E. B.; Molinero, V. *Phys. Chem. Chem. Phys.* **2011**, 13, 20008-20016.

(4) Moore, E. B.; Molinero, V. *Nature* **2011**, 479, 506-508.

(5) Song, B.; Molinero, V. *J. Chem. Phys.* **2013**, 139, 054511.

(6) Hudait, A.; Molinero, V. *J. Am. Chem. Soc.* **2014**, 136, 8081-8093.

(7) Jacobson, L. C.; Molinero, V. *J. Phys. Chem. B* **2010**, 114, 7302-7311.

(8) Naullage, P. M.; Molinero, V. in preparetion.

(9) Jorgensen, W. L.; Madura, J. D.; Swenson, C. J. *J. Am. Chem. Soc.* **1984**, 106, 6638-6646.

(10) Plimpton, S. *J. Comput. Phys.* **1995**, 117, 1-19.

(11) Nguyen, A. H.; Molinero, V. *J. Phys. Chem. B* **2015**, 119, 9369-9376.

(12) Hudait, A.; Qiu, S.; Lupi, L.; Molinero, V. *Phys. Chem. Chem. Phys.* **2016**, 18, 9544-9553.

(13) Graf, K.; Kappl, M. Physics and chemistry of interfaces; John Wiley & Sons, **2006**.

(14) D'Auria, R.; Tobias, D. J. *J. Phys. Chem. A* **2009**, 113, 7286-7293.

(15) Perez Sirkin, Y. A.; Factorovich, M. H.; Molinero, V.; Scherlis, D. A. *J. Chem. Theory Comput.* **2016**, 12, 2942-2949.

(16) Ogawa, S.; Koga, M.; Osanai, S. *Chem. Phys. Lett*. **2009**, 480, 86-89.

(17) Qiu, Y.; Odendahl, N.; Hudait, A.; Mason, R.; Bertram, A. K.; Paesani, F.; DeMott, P. J.; Molinero, V. *J. Am. Chem. Soc.* **2017**, 139, 3052-3064.

(18) Lupi, L.; Hudait, A.; Peters, B.; Grünwald, M.; Gotchy Mullen, R.; Nguyen, A. H.; Molinero, V. *Nature* 2017, under review.

(19) Turnbull, D. *J. Appl. Phys.* **1950**, 21, 1022-1028.

(20) Koop, T.; Luo, B.; Tsias, A.; Peter, T. *Nature* **2000**, 406, 611-614.

(21) Bullock, G.; Molinero, V. *Farad. Discuss.* **2013**, 167, 371-388.